Biomedical Signal Processing and Control 86 (2023) 105287

Contents lists available at ScienceDirect

Biomedical Signal Processing and Control

journal homepage: www.elsevier.com/locate/bspc

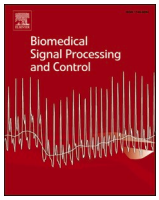

BPNet: A multi-modal fusion neural network for blood pressure estimation using ECG and PPG

Weicai Long, Xingjun Wang *

Department of Electronic Engineering, Tsinghua Shenzhen International Graduate School, Shenzhen, Guangdong 518055, China

ARTICLE INFO

Keywords:
Continuous blood pressure estimation
BoxCox transformation
Deep learning
Multi-modal fusion

ABSTRACT

This paper aims to address the problem of estimating blood pressure (BP) based on specific physiological signals. However, several issues exist in current works. Firstly, some methods produce biased models by training them on a skewed distribution and failing to consider the assumptions underlying regression analysis. Secondly, data leakage can occur when overlapping samples are present in the dataset. Finally, some methods concatenate Electrocardiogram (ECG) and Photoplethysmogram (PPG) signals without fully capturing their relationship. To overcome these limitations, this paper applies the BoxCox transformation to correct for skewed label distributions and creates a non-overlapping dataset. Additionally, a novel end-to-end model, the blood pressure network (BPNet), is proposed, which can accurately estimate blood pressure. The Multi-parameter Intelligent Monitoring in Intensive Care database (MIMIC) is utilized to develop and verify the model, which includes ECG, PPG, and invasive BP data from patients in intensive care units (ICUs). The BPNet is evaluated on the MIMIC II (942 subjects) and MIMIC-III (833 subjects) datasets. In MIMIC-II, the estimation error for systolic blood pressure (SBP) and diastolic blood pressure (DBP) is -0.17 ± 4.62 mmHg and -0.24 ± 2.95 mmHg, respectively. In MIMIC-III, the estimation error for SBP and DBP is -0.30 ± 5.78 mmHg and -0.25 ± 3.80 mmHg, respectively. The experimental results exceed the performance of existing methods and meet the accuracy standards established by the Association for the Advancement of Medical Instrumentation (AAMI) and the British Hypertension Society (BHS). This demonstrates the effectiveness and accuracy of the proposed model, highlighting the potential for practical applications in clinical settings.

1. Introduction

Hypertension is a medical condition that substantially raises the risk of heart, brain, kidney, and other diseases. According to the World Health Organization's 2022 statistical report, the number of individuals aged 30–79 years with hypertension has approximately doubled from 650 million to 1.28 billion between 1990 and 2019[1]. Early detection and diagnosis of abnormal blood pressure enable prompt treatment, potentially preventing the development of cardiovascular disease and reducing the risk of medication-related harm.

Techniques for measuring blood pressure are commonly categorized into invasive and non-invasive methods[2]. Invasive methods involve attaching a pressure transducer to an artery to measure blood pressure and are typically employed in significant surgeries to monitor a patient's physiological state continuously. Non-invasive methods, on the other hand, encompass both cuff-based and cuffless approaches. Cuff-based methods, such as the auscultation and oscillometric methods, rely on changes in vascular volume as indirect indicators of blood pressure. However, these methods can be uncomfortable and may cause skin irritation. Cuffless methods have been developed to overcome these issues, which fall into two categories: machine learning-based methods that use feature parameters and deep learning methods that take raw signals as input.

In recent years, researchers have increasingly explored deep learning methods for constructing blood pressure estimation models[3,4]. These methods offer the advantage of automatic feature extraction and improved estimation accuracy, which motivates this paper's adoption of deep learning methods. Nevertheless, this approach has three main drawbacks that must be addressed.

Firstly, some previous works have used only min–max or z-score normalization on the input[4,8] without considering the distribution of the labels. This can lead to biased models when training with skewed distributions, as illustrated in Fig. 1**(a)**. Specifically, regression analysis relies on the Mean Square Error (MSE) loss function, equivalent to

* Corresponding author.
E-mail address: wang.xingjun@sz.tsinghua.edu.cn (X. Wang).

https://doi.org/10.1016/j.bspc.2023.105287
Received 3 December 2022; Received in revised form 23 June 2023; Accepted 16 July 2023
Available online 5 August 2023

optimizing the Negative Log Likelihood (NLL). When training with a skewed distribution $P_{skew}(y)$, the resulting model $P_{train}(y|x)$ may not generalize well. To address this issue, we propose a transformation to convert the skewed distribution into a normal distribution $P_{gau}(y)$, which enables the training of an unbiased model. Here, λ and θ represent the parameters of the transformation and regressor, respectively.

Secondly, in the pre-processing step, some previous works allowed overlaps between adjacent samples[6,7], which led to a data leakage problem. Information from the test set may appear in the train set, thus allowing the model to perform well in the test set. As shown in Fig. 1**(b)**.

Finally, inadequate exploitation of physiological information may occur when ECG and PPG signals are concatenated without considering their implicit relationship, as illustrated in Fig. 1**(c)**. Such an approach has been previously employed, neglecting the potential benefits of fully capturing and utilizing physiological information.

This study aims to overcome the limitations of previous methods by introducing several novel techniques. Firstly, this paper employs the Box-Cox transformation to address the issue of skewed label distribution [9]. Additionally, this paper generates non-overlapping samples to prevent data leakage and proposes a novel deep learning architecture, BPNet, which effectively utilizes the information in ECG and PPG signals. The proposed model can produce highly accurate and dependable blood pressure estimations. Fig. 1 illustrates the comparison between skewed and normal distribution, data leakage, and no data leakage, as well as simple concatenation and our multi-modal fusion model.

In summary, this paper makes the following contributions:

(1) We revisited the problem of blood pressure regression and explored the effect of skewed distribution on the model's generalizability.
(2) There is no overlap between the data samples, which does not suffer from data leakage problems.
(3) BPNet is proposed as a cross-modal fusion method for blood pressure estimation. It can provide robust multi-modal feature representation for the task.

The paper is structured as follows: Section II provides a detailed overview of current works on blood pressure estimation using deep learning and machine learning techniques. Section III presents information on the dataset and the proposed BPNet architecture. Section IV presents the experimental results of BPNet based on international standards and comparisons with existing methods. Finally, in Section V, we conclude and consider future research directions.

2. Related work

This section reviews several lines of research related to our work in the following fields.

2.1. Imbalanced regression

Imbalanced regression has been a hot issue in recent research. Earlier works focus on resampling and synthesizing new samples for rare labels [10,11]. Later work ensembles the regressors obtained under different resampling policies[12]. Recent works have proposed to estimate the empirical training distribution using kernel density estimation (KDE) and then apply the standard reweighting technique[13,14]. In the field of computer vision, the regression task is usually given an image and outputs a label, where the labels are continuous. It requires that the test set be "balanced", which is also consistent with the goal of image regression model generalizability[15]. However, in the field of blood pressure estimation, the goal is to generalize to the population, which is inherently imbalanced and normally distributed from a statistical point of view. Therefore, the imbalance regression for blood pressure estimation requires an alternative view.

2.2. BP estimation using parameterized models

The ECG signal is a manifestation of the electrical activity of the heart muscle, mainly reflecting the contraction and diastole of the heart. QRS wave amplitude, QRS wave interval, ST-segment and T-wave features in ECG signals have been correlated with blood pressure.

The PPG signal is the propagation wave of blood through the blood vessels driven by the heart contraction, mainly reflecting the elasticity and hemodynamic state of the blood vessels. Since the stiffness and elasticity of blood vessels affect the pulse wave velocity (PWV), arterial blood pressure can be estimated indirectly.

Early works for cuffless BP estimation utilize the pulse transit time (PTT) or pulse arrival time (PAT)[16,17]. This approach is supported by Huges and Moens-Korteweg (MK) equation[18,19]. It assumes that blood is an incompressible, non-viscous fluid and that the vessel walls are thin and do not change in thickness or radius with changes in blood pressure. They subsequently validated a propagation model of ordinary fluids in elastic cavities through experimentation and used this to establish the relationship between PWV and vascular properties.

$$BP = \alpha \ln PAT + \beta \tag{2.1}$$

where α and β are experimentally calibrated constants, PAT is the only variable.

Both PTT and PAT were calculated from ECG and PPG. PTT is the time delay of the pulse propagation between two different arterial sites. PAT is the time delay between the electrical onset and the arrival of the evoked pulse wave at a specific site. PAT has an additional variable of the pre-ejection period (PEP) than PTT.

$$PAT = PTT + PEP \tag{2.2}$$

Since PEP is usually small, many works treat PAT and PTT as the same variable[20,21], and only a few works consider the effect of PEP on blood pressure[22,17].

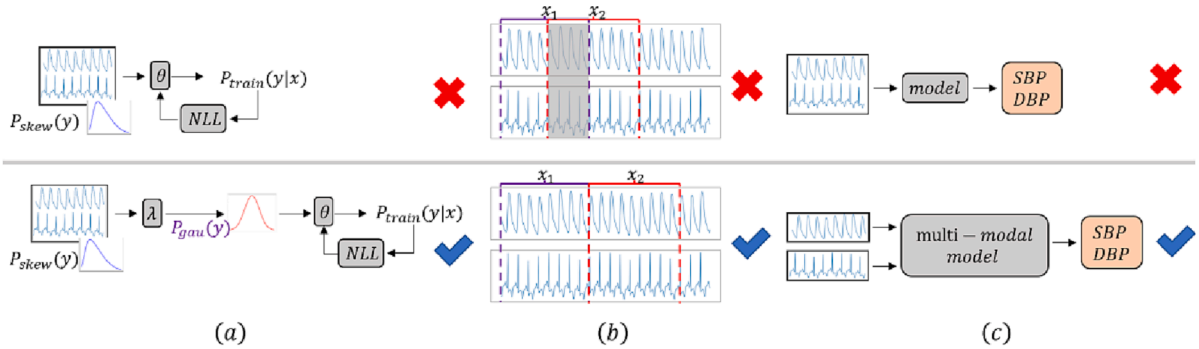

Fig. 1. Differences between this work and previous works.

In addition to PTT or PAT, some subsequent works focus on extracting features of ECG and PPG, including PPG first and second-order derivatives, pulse width, pulse amplitude, heart rate, and other features[23,24,25,26]. The general process is manually extracting these features based on physiological signals and then putting them into various machine learning models.

2.3. BP estimation using deep learning

In recent years, deep learning has rapidly grown, motivating many methods that use neural networks to estimate blood pressure.

In 2016, Sideris[27] et al. used 42 patients from the MIMIC-II dataset with a single-channel PPG as input to fit a true blood pressure curve via LSTM, and the final root mean square error of the fit was 6.042 ± 3.26 mmHg. In 2019, Slapničar[5] used the MIMIC-III dataset with a PPG as input and used ResNet to predict blood pressure changes relative to calibrated true values, with mean absolute errors of 9.43 and 6.88 for SBP and DBP, respectively. In 2020, Ibtehaz [4] used a single-channel PPG signal from the MIMIC-II dataset to input into U-Net to convert the PPG waveform into a blood pressure waveform, which received a B grade on the BHS standard. In 2018, Brian L. Hill [28]et al. instead used V-Net, where they collected ECG and pulse wave signals from 463 patients and ended up with errors of 2.398 ± 5.623 mmHg and −2.50 ± 3.79 mmHg for systolic and diastolic blood pressure, respectively. In 2022, Malayeri [29] transformed the PPG into a PPG recurrence plot. The PPG signal and PPG recurrence plot were fused to obtain the blood pressure output using a one-dimensional convolutional network and a two-dimensional convolutional network, respectively, with a final error of 3.05 ± 5.26 mmHg and 1.58 ± 2.60 mmHg for systolic and diastolic blood pressure, which achieved a better level.

In summary, blood pressure measurement methods can be divided into invasive and non-invasive methods. Non-invasive methods are further divided into methods using parameter models and deep learning methods. Their representative work and shortcomings are shown in Table 1.

3. Methodology

In this paper, we introduce a novel deep learning architecture, Blood Pressure Neural Network (BPNet), for continuous blood pressure estimation. The proposed method is illustrated in Fig. 2. Initially, we perform a preprocessing procedure that comprises quality assessment, signal filtering, and peak valley detection for the original ECG and PPG signals. The preprocessed ECG and PPG signals are then fed into BPNet, which consists of four components: pre-feature extraction, cross-modal fusion, post-feature extraction, and a multi-tasking module. The BPNet model outputs both SBP and DBP.

3.1. Revisiting regression task

We consider $x \in X, y \in Y = R^d$. MSE is the most commonly used loss function for regression problems. In fact, certain assumptions are applied to our task when we use a specific loss function. Under this assumption, the estimate of the sample set is derived from the maximum likelihood estimation before it is solved using convex optimization methods. From a statistical point of view, the relationship between the dependent variable y and the independent variable x satisfies the following:

$$y^{(i)} = \theta^T x^{(i)} + \epsilon^{(i)} \tag{3.1}$$

where θ is the regressor's parameter, $\epsilon^{(i)}$ is the residual term. In general, we assume that the residual terms in the linear regression conform to a normal distribution[31].

$$p\left(\epsilon^{(i)}\right) = N\left(0, \sigma^2\right) \tag{3.2}$$

where σ is the scale of an i.i.d. error term. Substituting Eq. (3.1) into Eq. (3.2), we can obtain

$$p\left(y^{(i)}|x;\theta\right) = N\left(y^{(i)}; y^{(i)}_{pred}, \sigma^2\right) \tag{3.3}$$

Our goal is to optimize the Eq. (3.3). It is easy to show that MSE equals to the Negative Log Likelihood (NLL) loss[32] of the prediction distribution $p\left(y^{(i)}|x;\theta\right)$. Taking the logarithm of both sides of Eq. (3.3), we get.

$$\begin{aligned} \log L(\theta) &= \sum_{i=1}^{n} log \frac{1}{\sqrt{2\pi}\sigma} exp\left(-\frac{\left(y^{(i)} - y^{(i)}_{pred}\right)^2}{2\sigma^2}\right) \\ &= \&n\log\frac{1}{\sqrt{2\pi}\sigma} - \frac{1}{\sigma^2}\cdot\frac{1}{2}\sum_{i=1}^{n}\left(y^{(i)} - y^{(i)}_{pred}\right)^2 \end{aligned} \tag{3.4}$$

The first term on the right side of Eq. (3.4) is a constant. The overall likelihood function has to take the maximum value, so the second term has to be as small as possible, so we have.

$$J(\theta) = \left\|y^{(i)} - y^{(i)}_{pred}\right\|_2^2 \tag{3.5}$$

where $\|\cdot\|_2$ denotes L_2 norm. Eq. (3.5) is the expression of MSE. In summary, for the task of blood pressure estimation, the label distribution must be normal.

Normally, both the training and test set are sampled from the same joint distribution. However, when the label distribution is highly skewed, the model can learn a trivial solution by always predicting frequent labels. In this case, the model may give up "thinking" and act as a guessing tool instead[33]. To solve this problem, we transform the original data with significant skewness into a normal distribution by preprocessing so that the MSE can be used as a loss function for optimization. We use the Box-Cox transformation, which converts the skewed distribution into a normal distribution using the parameter λ.

$$\widehat{y} = \begin{cases} \dfrac{y^{\lambda} - 1}{\lambda}, \lambda \neq 0 \\ \ln y, \lambda = 0 \end{cases} \tag{3.6}$$

where $\widehat{y}$ is the new variable obtained by Box-Cox transformation. y is the original continuous dependent variable and λ is the transformation parameter, which can be solved by maximum likelihood estimation.

Table 1
Drawbacks of the existing systems.

Category	Method	Representative work	Drawback
Invasive	/	/	High prices and causing trauma
Non-invasive	Auscultation	Laennec et al. [30]	Different doctors have significant errors
	Parameterized model	Ding et al. [16]	Complex feature extraction steps
	Deep learning	Kachuee et al. [35]	Skewed distribution and Low accuracy

3.2. Data preprocessing

The MIMIC-II dataset is available in a compiled version but may still contain anomalies such as long blank or missing data segments. These anomalous segments must be removed through additional screening. On the other hand, the MIMIC-III database is completely uncompiled. Consequently, our preprocessing process involves three steps: quality assessment, signal filtering, and peak valley detection.

Quality Assessment: The ECG, PPG, and arterial blood pressure (ABP) signals are subject to various types of noise in the human body,

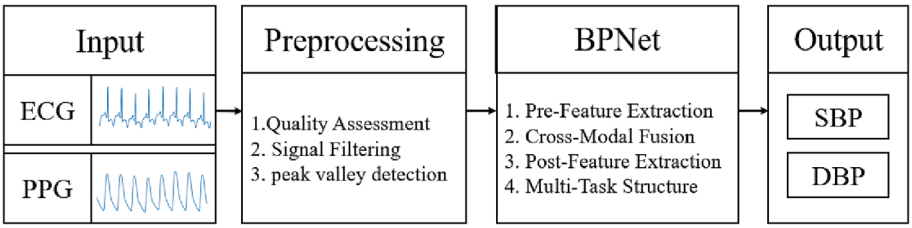

Fig. 2. Block diagram of the proposed approach.

such as blank signals, baseline drift, high-frequency electromyography (EMG), and abnormal impulses. Removing blank and abnormal signals using filtering alone is challenging, so we resort to segment removal. We propose a quality assessment rule to ensure that only segments containing useful information are removed. This rule improves the reliability of the results by filtering out only the segments that do not contain any relevant information.

(1) To address the blank signals present in ECG, PPG, and arterial blood pressure (ABP) signals, we propose fixing a window of 3000 sample points and performing a quality assessment on these segments.
(2) We evaluate the PPG, ECG, and ABP signals based on the range of signal amplitude and the number of signal derivatives with 0. Under normal conditions, the range of these signals is limited. Therefore, signals beyond this range are considered abnormal. Additionally, by determining the number of derivatives with 0, we can identify the presence of blank signals within a segment.

Signal Filtering: We use different filtering methods for ECG and PPG signals to remove noise from the raw signal.

(1) For PPG, the prominent noise is baseline drift, which is eliminated using the db8 wavelet. We decompose the original signal into 8 levels by discrete wavelet transformation[36] and use the "Sureshrink" threshold rule. It is based on minimizing the estimated signal's mean squared error while setting small wavelet coefficients to zero. This helps to remove noise while preserving the valuable signal components.
(2) For ECG, the prominent noise is baseline drift and EMG interference. Baseline drift is a low-frequency noise, while EMG interference is a high-frequency noise. We use a bandpass filter with a passband of 1 Hz to 35 Hz to eliminate these noises.

Peak Valley Detection: To better obtain the true values corresponding to the samples, we use the slope sum function (SSF) to detect the peaks and valleys of the ABP signal[37]. The purpose of the SSF function is to enhance the rising slope of the waveform and suppress the falling slope. At time i, the window weighting z_i is defined as follows:

$$z_i = \sum_{k=i-w}^{i} \Delta u_k, \Delta u_k = \begin{cases} \Delta y_k, \Delta y_k > 0 \\ 0, \Delta y_k \le 0 \end{cases} \tag{3.7}$$

where w is the window length, and N is the number of signal sampling points, $\Delta y_k = y_k - y_{k-1}$. w is generally chosen as the length of the signal rise slope. Fig. 3 shows the effect of BP signal wave detection based on SSF. The above figure shows the ABP signal. The red points denote the peaks, and the green points denote the valleys. The lower figure is the transformed SSF signal. The green point denotes the "onset" point, which corresponds to the valley point of ABP.

After obtaining the peak and valley values, we calculate the average values as the true values of SBP and DBP corresponding to the samples, respectively.

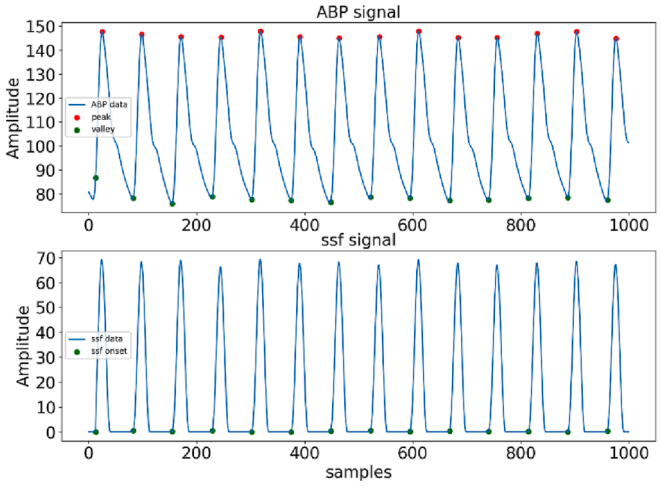

Fig. 3. Detection of wave peaks and valleys based on SSF.

3.3. *BPNet architecture*

Fig. 4 illustrates the architecture of our proposed model. We first utilize two separate Convolutional Neural Networks (CNNs) to extract diverse levels of visual feature maps from the PPG and ECG signals. These maps are then mapped to the corresponding shared space and fused at the channel level to generate multi-modal feature maps for each signal. These multi-modal feature maps enable the representation of each PPG and ECG signal. Next, we introduce the feature pyramid network (FPN) [38] to fuse the information of the multi-modal feature maps at various scales, enhancing the semantic and positional information of the PPG and ECG signals to capture their physiological morphology. To eliminate the confounding effect caused by upsampling, we perform another convolution after the FPN features are fused. Using the same convolutional structure, the smoothed multi-modal features extract the feature information corresponding to systolic blood pressure (SBP) and diastolic blood pressure (DBP), respectively. The post-feature extraction module shares information between the two tasks and ultimately learns the representation associated with SBP and DBP to obtain the blood pressure values.

Our model is motivated by several observations. Firstly, the method based on Pulse Transit Time (PTT) or Pulse Arrival Time (PAT) is supported by the Moens-Korteweg (MK) equation. These two parameters are calculated from the ECG and PPG signals. Therefore, it is necessary to use both the ECG and PPG signals in our model.

Secondly, we prioritize waveform features over temporal relationships. While previous works have utilized Long Short-Term Memory (LSTM)[27] networks to extract temporal relationships and predict future blood pressure values based on past data, our goal is to estimate blood pressure values based on physiological signals. Therefore, our model architecture uses Convolutional Neural Networks (CNNs) over LSTMs.

Thirdly, Existing methods for blood pressure estimation have limitations in terms of accuracy, which led us to develop a new approach.

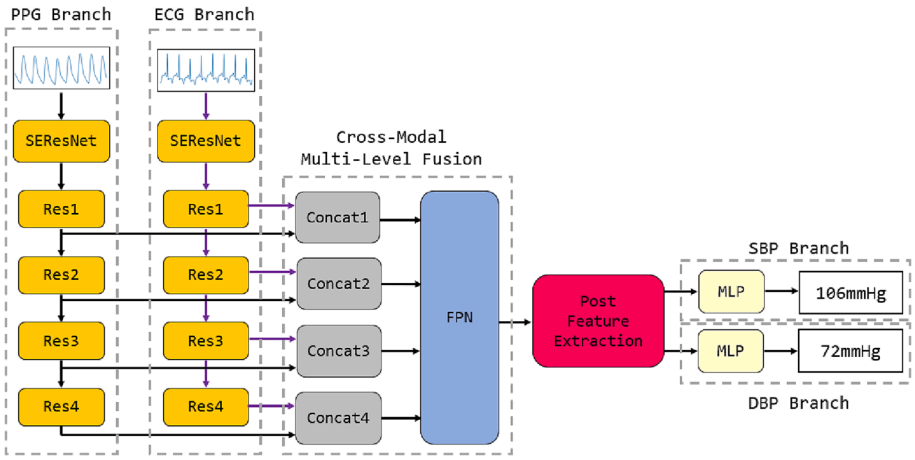

Fig. 4. Overview of BPNet.

Previous works[39,40] have concatenated ECG and PPG signals together for this task, but this simple modal fusion approach overlooks important details for blood pressure estimation. To overcome this limitation, we introduced a cross-modal multi-level fusion module that enables information exchange between the two modalities at different levels, better capturing relevant details and improving accuracy.

Finally, the blood pressure estimation task is a complex multi-task problem. In previous works[41,42], it was common to train separate networks to estimate systolic blood pressure (SBP) and diastolic blood pressure (DBP). However, recent studies[40,43] have shown that a multi-task approach could provide better performance in terms of accuracy and efficiency. Therefore, we adopt a multi-task structure in our model to estimate SBP and DBP simultaneously.

(1) Cross-Modal Multi-level fusion

The input consists of a segment of the PPG signal and a segment of the ECG signal, and we first extract the visual features of PPG and ECG using a CNN as the backbone, respectively. The feature map extracted from a particular CNN layer can be expressed as $V \in R^{C\times L}$, where C and L are the dimensions of channel and length.

After extracting the features, we construct four joint multi-modal feature-sharing subspaces to fuse PPG and ECG multi-level features in the channel dimensions. We use $V_{ppg}, V_{ecg} \in R^{C}$ to denote the visual feature vector of PPG and ECG. We can define multi-modal features corresponding to specific levels of ECG and PPG as follows:

$$f_p = Concat\left(\frac{V_{ppg}}{\|V_{ppg}\|_2}, \frac{V_{ecg}}{\|V_{ecg}\|_2}\right) \tag{3.8}$$

Where $\|\cdot\|_2$ denotes the L_2 norm and Concat(·) denotes the concatenation of two feature vectors in the channel dimension. The feature vector f_p fuses the multi-level visual features of PPG and ECG to achieve the role of encoding visual information with dimension ($C_{ppg} + C_{ecg}$).

To address the issue of initially obtained cross-modal features containing redundant information, we implemented the FPN for modal fusion. FPN equalizes the number of channels across all feature maps, reducing redundant information for higher-level feature maps. This allows the semantic information of the deep network to be fused into the shallow location information, thereby guiding the network to estimate blood pressure based on location and semantics. As illustrated in Fig. 5, we slightly modified the original FPN by only utilizing the last layer of the fused feature map. The feature map is the largest and can focus on more minor waveform details. The 1x1 convolution is denoted by "Conv" and the element-wise summation is denoted by ⊕.

(2) Post Feature Extraction

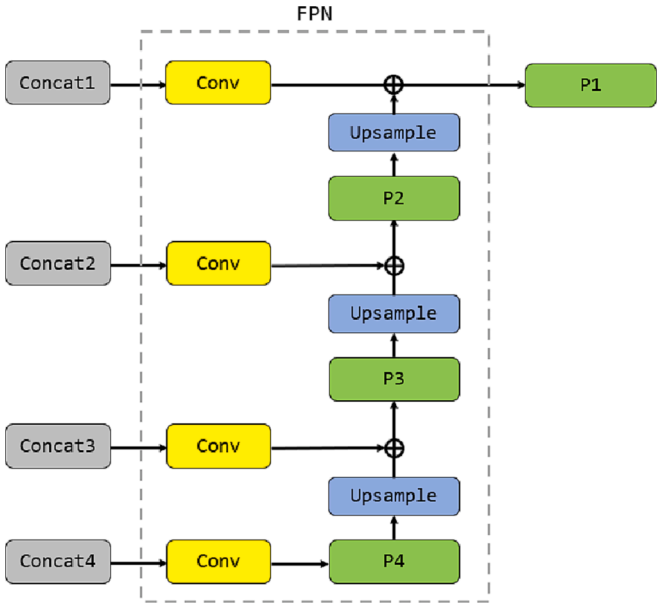

Fig. 5. Illustration of the fusion process of ECG and PPG features.

The features fused by FPN are in the shared space, which may lead to excessive parameter sharing if applied directly to the subsequent SBP and DBP estimation tasks. To avoid this, we perform further feature extraction on the fused features. Fig. 6 illustrates this process, where we first use a convolutional layer for smoothing and then two convolutional layers to extract features. The output is the shared features, which are then used for SBP and DBP estimation tasks. The white conv module represents a 3x3 convolution with a stride of 1, while the light blue module represents a 3x3 convolution with a stride of 2.

(3) Multi-task structure

Our model performs multi-level feature fusion of ECG and PPG, followed by adding a three-layer CNN to extract the fused features. The rationale for this approach is two-fold: Firstly, the fused features obtained from multi-level fusion often need to be more stable. Secondly, adding the CNN layers allows for stable parameter sharing between the two tasks, which introduces noise from the other task and improves the generalization effect (see Table 2).

In addition, if the loss functions of two tasks differ significantly, the overall model will prefer a task. To solve this problem, we carefully

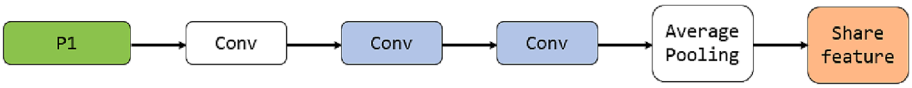

Fig. 6. Illustration of the post-feature extraction process.

Table 2
Descriptions of MIMIC-II and MIMIC-III dataset.

		MIMIC-II	MIMIC-III
Cleaning required		No	Yes
Patients		942	833
Sample length		10 s	
Total samples		245,638	8,330,000
Train set samples		157,208	533,120
Validate set samples		39,303	133,280
Test set samples		49,127	166,600
SBP	Range(mmHg)	80–180	80–180
	Skewed	No	No
DBP	Range(mmHg)	50–110	30–110
	Skewed	Yes	No

designed the loss function:

$$Loss = \frac{1}{n}\sum_{i}^{n}\left[\left(SBP_{pi} - SBP_{ti}\right)^2 + corrcoef * \left(DBP_{pi} - DBP_{ti}\right)^2\right] \tag{3.9}$$

where *corrcoef* is the scaling factor.

$$corrcoef = \frac{\left(SBP_{pi} - SBp_{ti}\right)^2}{\left(DBP_{pi} - DBP_{ti}\right)^2} \tag{3.10}$$

This ensures that the loss value is the same for both tasks. Our SBP and DBP network branches consist of two separate multi-layer perceptron (MLP) modules, which consist of two linear layers to estimate the final blood pressure values (see Table 3).

4. Experiment

In this section, we evaluate the performance of our proposed method. We introduce the dataset in Section 4.1, an indispensable component of our experiments. Moving on to Section 4.2, we carefully delineate the experiment-related setup. The evaluation metrics that we employ to assess our model's performance accurately in Section 4.3 provide us with valuable insights into the efficacy of our method. In Section 4.4, we present the main results of our study, which are obtained by meticulously analyzing and comparing our approach with recent studies. We conclude our experiment by conducting a detailed ablation experiment in Section 4.5, which meticulously illustrates the relevant contributions of each component of our proposed method.

4.1. Dataset

Multi-parameter Intelligent Monitoring in Intensive Care (MIMIC) database contains time series of physiological signals and vital signs acquired from ICU patients[34], with a uniform sampling rate of 125 Hz. However, the compiled version of MIMIC-III is currently not available. In our experiments, we used MIMIC-II compiled by Kachuee et al.[35] and MIMIC-III compiled by ourselves, containing 942 subjects (245,638 samples) and 833 subjects (833,000 samples), respectively.

Table 3
Comparison of this study with other works in MIMIC-II.

Method	label	ME↓	MAE↓	STD↓	r↑
No Box-Cox	SBP	−0.16	4.15	4.68	0.9540
	DBP	**−0.23**	2.57	2.99	0.9273
No fusion	SBP	−0.63	4.65	5.37	0.9407
	DBP	−0.71	2.69	3.38	0.9137
Single task	SBP	**−0.15**	4.38	4.77	0.9506
	DBP	−0.34	2.57	3.14	0.9229
2D Regression	SBP	−0.89	4.71	4.92	0.9464
	DBP	−0.28	2.68	3.27	0.9165
ours	SBP	−0.17	**3.98**	**4.62**	**0.9564**
	DBP	−0.24	**2.33**	**2.95**	**0.9340**

4.2. Implementation details

The MIMIC-II dataset formed after preprocessing has 942 patients with 245,638 samples. The MIMIC-III dataset has 833 patients, with 1000 samples taken from each patient, for a total of 833,000 samples. We operate on both datasets separately, randomly selecting 64% of the samples as the train set, 16% as the validation set, and the remaining 20% as the test set.

We use the deep learning framework PyTorch to train the model, running on the Ubuntu 16.04.1 LTS operating system. The server configuration is 4-way 3090 GPUs with 24G memory on each card. In addition to this, the server has a 10-core Xeon silver 4210 CPU and 128 GB of RAM.

Our segment length is chosen to be 10 s (1250 samples) without any overlap between samples. The labels are the means of all peaks and valleys within a given segment.

$$\begin{aligned} SBP &= \&mean(SBP_i) \\ DBP &= \&mean(DBP_i) \end{aligned} \tag{3.11}$$

where SBP_i and DBP_j are the detected values of peak and valley within a given segment, respectively. Given a 10-second PPG signal and an ECG signal, we use the output of the SEResNet Block as input for the multi-modal features. The channel dimension used for FPN feature fusion is two times the initial model width of SE-ResNet. The network is trained using an initial learning rate of 1e-3. When the evaluation metric stops improving by two epochs, the learning rate is reduced to 0.2 times of the original one, and the minimum learning rate is set to 1e-5.

4.3. Metrics

(1) BHS Standard

The British Hypertension Society (BHS)[44] has put forward a comprehensive evaluation scheme for assessing the accuracy of blood pressure measurement devices and methods. The evaluation scheme is based on a discrete assessment criterion that considers the percentage of cumulative error as a measure of performance accuracy. The evaluation is divided into different classes, each with its specific threshold for the percentage of cumulative error. To be awarded a specific class, the cumulative percentage error of a method must exceed the threshold for the specific class in each of the three categories, namely 5 mmHg, 10 mmHg,

Table 4
Evaluation using BHS standard.

		Cumulative Error Percentage			
		<5mmHg	<10 mmHg	<15 mmHg	Grade
MIMIC-II	SBP	74.47%	92.52%	97.05%	**A**
	DBP	89.57%	97.70%	99.13%	**A**
MIMIC-III	SBP	59.47%	84.90%	93.73%	**B**
	DBP	79.90%	95.01%	98.24%	**A**
BHS	Grade A	60%	85%	95%	
	Grade B	50%	75%	90%	
	Grade C	40%	65%	85%	

and 15 mmHg. The details of the evaluation scheme and the specific thresholds for each class are summarized in Table 4.

(2) **AAMI Standard**

The AAMI[45] standard is similar to the BHS standard in that it also provides a set of rules to evaluate the accuracy of blood pressure measurement devices and methods. According to the AAMI standard, the assessment criteria are based on whether the mean error (ME) and standard deviation (STD) are within the range of 5 mmHg and 8 mmHg. However, unlike the BHS standard, the AAMI criteria only apply to evaluating methods involving at least 85 subjects participating in the blood pressure assessment. As shown in Table 5.

(3) **Metrics for Regression Models**

In this paper, four evaluation metrics are used to evaluate the proposed model, including Pearson correlation coefficient r, mean error (ME), mean absolute error (MAE), and standard deviation (STD). The r measures the agreement between the estimated and true values, and the ME measures the error between the estimated and true values, the MAE measures the absolute error between the estimated and true values, and the STD measures the deviation from the ME. The four metrics are defined as follows:

$$r = \frac{\sum_{i=1}^{n}(y_i - \bar{y})(\hat{y}_i - \bar{\hat{y}})}{\sqrt{\sum_{i=1}^{n}(y_i - \bar{y})^2}\sqrt{\sum_{i=1}^{n}(\hat{y}_i - \bar{\hat{y}})^2}} \tag{3.12}$$

$$ME = \frac{1}{n}\sum_{i=1}^{n}(\hat{y}_i - y_i) \tag{3.13}$$

$$MAE = \frac{1}{n}\sum_{i=1}^{n}|\hat{y}_i - y_i| \tag{3.14}$$

$$STD = \sqrt{\frac{\sum_{i=1}^{n}(\hat{y}_i - y_i - ME)^2}{n-1}} \tag{3.15}$$

where y_i is the true value extracted from the ABP, $\hat{y}_i$ is the estimated value of the model, and n is the number of samples in the test set.

4.4. Ablation study

We perform ablation experiments on the MIMIC-II dataset to further investigate the relative contribution of each component of our model.

(1) **Box-Cox transformation**

The labels in our dataset exhibit a skewed distribution, which can negatively impact the performance of the regression model. Therefore, we utilize the Box-Cox transformation to convert the skewed distribution to a normal distribution. As demonstrated in Table 9, the model trained on the preprocessed data with Box-Cox transformation yields better results than the model without the skew correction. This highlights the importance of transforming the data to a normal distribution when using the MSE loss function for regression analysis.

Table 5
Evaluation using AAMI standard.

		ME	STD	Passed
MIMIC-II	SBP	−0.17	4.62	**Y**
	DBP	−0.24	2.95	**Y**
MIMIC-III	SBP	−0.30	5.78	**Y**
	DBP	−0.25	3.80	**Y**
AAMI	>=85 subjects	<=5	<=8	

(2) **Cross-modal multi-level feature fusion**

In this experiment, the effectiveness of multi-modal fusion is evaluated by comparing the method of directly using two-channel ECG and PPG with the method of mapping features to a shared space for fusion. As shown in Table 9, the fusion method is more effective than the no-fusion method.

(3) **Multi-task blood pressure estimation**

This experiment aims to confirm the impact of the multi-task structure on the model's performance. The single-task structure is inefficient. 2D regression leads to problems with a model preference for tasks. In contrast, the multi-task structure facilitates parameter sharing, allowing the model to learn related tasks simultaneously. According to Table 9, the multi-task structure model outperforms the other models.

4.5. Evaluation results

In the MIMIC-II dataset, the correlation coefficient (r) for SBP and DBP are 0.9564 and 0.9340, respectively. The mean error (ME) ± standard deviation (STD) are −0.17 ± 4.62 mmHg and −0.24 ± 2.95 mmHg, respectively. Additionally, the mean absolute error (MAE) of SBP and DBP are 3.98 mmHg and 2.33 mmHg, respectively. Fig. 7 **and** Fig. 8 show the correlation and Bland-Altman plots.

The correlation plot depicts the estimated BP values against the true BP values, with the x-axis representing the true value and the y-axis representing the estimated value. Most of the points are close to the black line, indicating a strong correlation between the estimated and true values.

In the Bland-Altman plot, the x-axis represents the BP mean, defined as the average of the estimated and true values, while the y-axis shows the difference between the estimated and true values. The plot illustrates the deviation ME with the allowed limit, with over 95% of the points falling within the two red lines. This suggests a high correlation between the estimated and true values, indicating the accuracy of the estimation.

Tables 4 and 5 show the performance of BPNet based on BHS and AAMI. On the BHS standard, it can be seen that MIMIC-II has achieved a grade A for both SBP and DBP. MIMIC-III has achieved a grade of B for SBP and an A for DBP. On the AAMI standard, the errors of BPNet are met on both datasets.

(1) **Running Time**

As shown in Table 6, in the MIMIC-II dataset, our test set consisted of 49,127 samples, and the time consumed by a single GPU was approximately 103 s, with a testing time of approximately 0.002 s per sample. The CPU consumed 1250 s, with a testing time of approximately 0.03 s per sample.

In the MIMIC-III dataset, our test set consisted of 166,600 samples, and the time consumed by a single GPU was approximately 499 s, with a testing time of approximately 0.003 s per sample. The CPU consumed 4998 s, with a testing time of approximately 0.03 s per sample.

(2) **Comparison of different segment length**

To illustrate and validate the robustness of the model, we conducted many experiments during the initial period and found that the model is not very sensitive to some change such as sample length, and the detailed data are as shown in Table 7.

It can be seen that different segment length have little effect on the model.

(3) **Comparison of other deep learning methods**

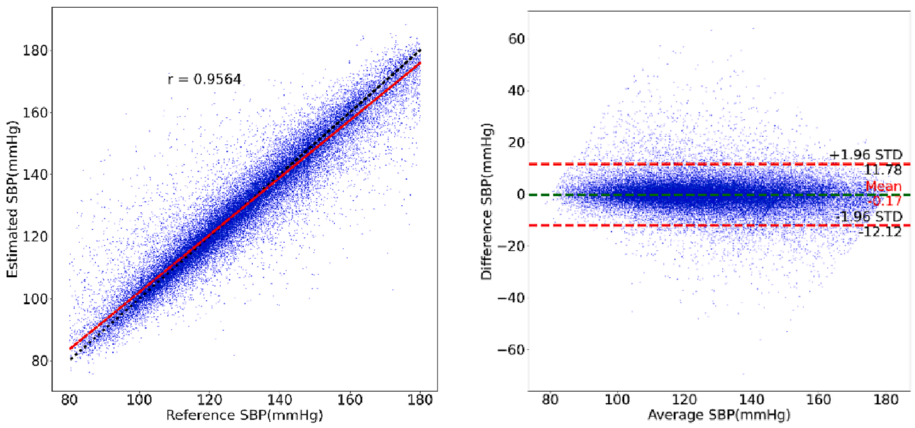

Fig. 7. Correlation plots and Bland-Altman plots of SBP on the MIMIC-II dataset.

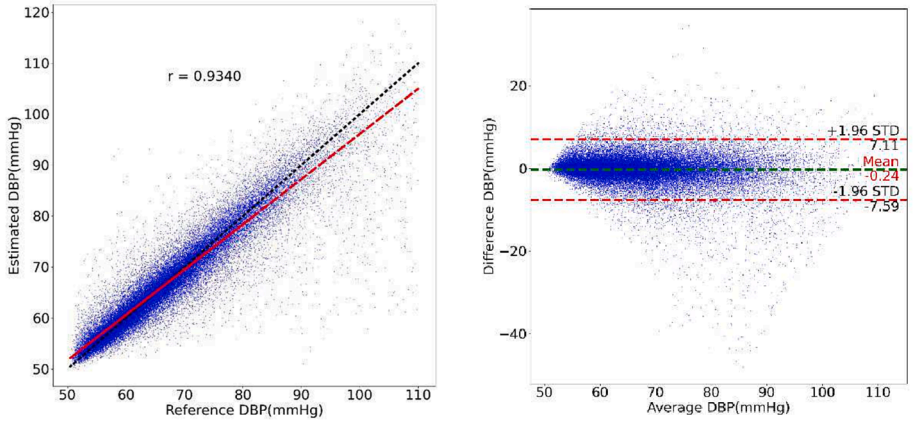

Fig. 8. Correlation plots and Bland-Altman plots of DBP on the MIMIC-II dataset.

Table 6
Running time of BPNet in the MIMIC-II and MIMIC-III dataset.

	Test samples	GPU time (all)	GPU time (per)	CPU time (all)	CPU time (per)
MIMIC-II	49,127	103 s	0.002 s	1250 s	0.03 s
MIMIC-III	166,600	499 s	0.003 s	4998 s	0.03 s

Table 8 and 9 compare the proposed deep learning model with other models using default parameters, including ResNet18, SEResNet18, and LSTM. The hyperparameters of all models are the same for a fair comparison. The results show that the proposed model outperforms the others in all metrics except the ME metric.

(4) **Comparison of other works**

To demonstrate the superior performance of the model proposed in this paper, a comparison is made with recent works in Table 10 and Table 11. The results indicate that our method outperforms other approaches in almost all metrics. Additionally, it is worth noting that we use the most reasonable way of composing the MIMIC-III dataset, i.e., each patient contributed the same number of samples. Overall, the proposed model has achieved comprehensive improvements in all metrics, making it a more reliable and effective approach for blood pressure estimation.

5. Conclusion

This paper addresses previous shortcomings in blood pressure estimation, including label distribution and underutilization of ECG and PPG information. The proposed method employs Box-Cox transformation to normalize skewed distributions and create non-overlapping samples to address these challenges. BPNet, a novel deep

Table 7
Comparison of different segment length in MIMIC-II.

Segment length	SBP				DBP			
	ME	MAE	STD	r	ME	MAE	STD	r
5 s	−0.04	4.1	4.76	0.9545	−0.71	2.63	3.14	0.9296
8 s	−0.16	3.93	4.71	0.9564	−0.02	2.38	2.97	0.9325
12 s	0.20	4.62	5	0.9472	−0.07	2.7	3.14	0.9199
15 s	−0.39	4.44	4.94	0.9496	−0.03	2.54	3.04	0.9249
ours (10 s)	−0.17	3.98	4.62	0.9564	−0.24	2.33	2.95	0.9340

Table 8
Comparison of the results of different methods on MIMIC-II.

Method	SBP				DBP			
	ME↓	MAE↓	STD↓	r↑	ME↓	MAE↓	STD↓	r↑
ResNet18	−0.18	5.12	5.37	0.9350	−0.39	2.93	3.44	0.9035
SEResNet18	−0.62	4.60	5.26	0.9428	−0.69	2.68	3.33	0.9154
LSTM	−0.25	13.45	10.66	0.5690	**−0.18**	6.73	5.68	0.5431
ours	**−0.17**	**3.98**	**4.62**	**0.9564**	−0.24	**2.33**	**2.95**	**0.9340**

Table 9
Comparison of the results of different methods on MIMIC-III.

Method	SBP				DBP			
	ME↓	MAE↓	STD↓	r↑	ME↓	MAE↓	STD↓	r↑
Resnet34	−0.12	6.67	6.81	0.8996	−0.26	4.02	4.38	0.8975
SERes34	−0.29	5.82	6.15	0.9217	−0.31	3.50	3.98	0.9191
LSTM	**0.11**	15.73	11.63	0.4353	**0.05**	9.30	7.31	0.4709
ours	−0.30	**5.59**	**5.78**	**0.9295**	−0.25	**3.35**	**3.80**	**0.9265**

Table 10
Comparison with other works in MIMIC-II.

	Subjects	SBP				DBP			
		ME↓	MAE↓	STD↓	r↑	ME↓	MAE↓	STD↓	r↑
[3]	942	−0.23	5.16	8.50	–	0.59	2.89	4.78	–
[4]	942	−1.58	5.73	10.69	–	1.62	3.45	6.86	–
[8]	1227	1.65	5.42	6.64	–	−1.28	3.14	3.74	–
[46]	942	−0.29	7.83	9.10	–	**−0.09**	4.86	5.21	–
[47]	942	–	5.32	5.54	–	–	3.38	3.82	–
ours	942	**−0.17**	**3.98**	**4.62**	**0.9564**	−0.24	**2.33**	**2.95**	**0.9340**

Table 11
Comparison with other works in MIMIC-III.

	Subjects	SBP				DBP			
		ME↓	MAE↓	STD↓	r↑	ME↓	MAE↓	STD↓	r↑
[26]	1711	**−0.11**	7.10	9.99	0.88	0.01	4.61	6.29	0.71
[5]	510	–	9.43	–	–	–	6.88	–	–
[35]	57	–	8.21	5.45	0.54	–	4.31	**3.52**	0.57
[47]	23	–	8.70	–	–	–	4.60	–	–
[48]	264	4.30	–	6.53	–	−3.11	–	4.57	–
ours	833	−0.30	**5.59**	**5.78**	**0.9295**	**−0.25**	**3.35**	3.80	**0.9265**

learning architecture, is introduced for continuous blood pressure estimation. BPNet can effectively capture the relationship between ECG and PPG at different levels. In comparison to previous works, BPNet achieves superior performance. Overall, this work provides a promising solution for blood pressure estimation, which may facilitate the widespread clinical application of wearable devices.

Funding

This work is partly supported by the Shenzhen Science and Technology Innovation Commission (No.KCXFZ202002011010487) and the Key Project of Stable Funding for Higher Education Institutions (No. WDZC20200818121348001).

CRediT authorship contribution statement

Weicai Long: Conceptualization, Methodology, Software, Data curation, Writing – original draft, Visualization, Investigation, Supervision, Software, Validation. **Xingjun Wang:** Conceptualization, Funding acquisition, Resources, Supervision, Writing – review & editing.

Declaration of Competing Interest

The authors declare that they have no known competing financial interests or personal relationships that could have appeared to influence the work reported in this paper.

Data availability

Data will be made available on request.

References

[1] World health statistics 2022: monitoring health for the SDGs, sustainable development goals. Geneva: World Health Organization; 2022. Licence: CC BY-NC-SA 3.0 IGO.
[2] M. Cepeda, P. Pham, D. Shimbo, Status of ambulatory blood pressure monitoring and home blood pressure monitoring for the diagnosis and management of hypertension in the US: an up-to-date review, Hypertens. Res. 46 (3) (2023) 620–629.
[3] K.R. Vardhan, S. Vedanth, G. Poojah, et al., BP-Net: Efficient Deep Learning for Continuous Arterial Blood Pressure Estimation using Photoplethysmogram, in: 2021 20th IEEE International Conference on Machine Learning and Applications (ICMLA), 2021, pp. 1495–1500.

[4] N. Ibtehaz, S. Mahmud, M.E.H. Chowdhury, et al. Ppg2abp: Translating photoplethysmogram (ppg) signals to arterial blood pressure (abp) waveforms using fully convolutional neural networks. arXiv preprint arXiv:2005.01669, 2020.
[5] G. Slapničar, N. Mlakar, M. Luštrek, Blood pressure estimation from photoplethysmogram using a spectro-temporal deep neural network, Sensors 19 (15) (2019) 3420.
[6] T. Athaya, S. Choi, An estimation method of continuous non-invasive arterial blood pressure waveform using photoplethysmography: A U-Net architecture-based approach, Sensors 21 (5) (2021) 1867.
[7] M.A. Mehrabadi, S.A.H. Aqajari, A.H.A. Zargari, et al., Novel blood pressure waveform reconstruction from photoplethysmography using cycle generative adversarial networks, in: 2022 44th Annual International Conference of the IEEE Engineering in Medicine & Biology Society (EMBC). IEEE, 2022, pp. 1906–1909.
[8] K. Qin, W.u. Huang, T. Zhang, Deep generative model with domain adversarial training for predicting arterial blood pressure waveform from photoplethysmogram signal, Biomed. Signal Process. Control 70 (2021) 102972.
[9] X.-S. Si, T. Li, J. Zhang, Y. Lei, Nonlinear degradation modeling and prognostics: A Box-Cox transformation perspective, Reliab. Eng. Syst. Saf. 217 (2022) 108120.
[10] P. Branco, L. Torgo, R.P. Ribeiro, SMOGN: a pre-processing approach for imbalanced regression[C]//First international workshop on learning with imbalanced domains: Theory and applications, PMLR (2017) 36–50.
[11] L. Torgo, R.P. Ribeiro, B. Pfahringer, et al. Smote for regression, in: Progress in Artificial Intelligence: 16th Portuguese Conference on Artificial Intelligence, EPIA 2013, Angra do Heroísmo, Azores, Portugal, September 9-12, 2013. Proceedings 16. Springer Berlin Heidelberg, 2013: 378-389.
[12] P. Branco, L. Torgo, R.P. Ribeiro, Rebagg: Resampled bagging for imbalanced regression, in: Second International Workshop on Learning with Imbalanced Domains: Theory and Applications. PMLR, 2018, pp. 67–81.
[13] Y. Yang, K. Zha, Y. Chen, et al. Delving into deep imbalanced regression, in: International Conference on Machine Learning. PMLR, 2021: 11842-11851.
[14] M. Steininger, K. Kobs, P. Davidson, A. Krause, A. Hotho, Density-based weighting for imbalanced regression, Mach. Learn. 110 (8) (2021) 2187–2211.
[15] J. Ren, M. Zhang, C. Yu, et al., Balanced mse for imbalanced visual regression, in: Proceedings of the IEEE/CVF Conference on Computer Vision and Pattern Recognition, 2022, pp. 7926–7935.
[16] H. Shin, A novel method for non-invasive blood pressure estimation based on continuous pulse transit time: An observational study, Psychophysiology 60 (2) (2023) e14173.
[17] Z.B. Zhou, T.R. Cui, D. Li, et al. Wearable continuous blood pressure monitoring devices based on pulse wave transit time and pulse arrival time: a review. Materials, 2023, 16(6): 2133.
[18] MA. Isebree, Die Pulscurve. Leiden, the Netherlands: EJ Brill, 1878.
[19] X. Quan, J. Liu, T. Roxlo, S. Siddharth, W. Leong, A. Muir, S.-M. Cheong, A. Rao, Advances in non-invasive blood pressure monitoring, Sensors 21 (13) (2021) 4273.
[20] R. Shriram, A. Wakankar, N. Daimiwal, et al. Continuous cuffless blood pressure monitoring based on PTT, in: 2010 International Conference on Bioinformatics and Biomedical Technology. IEEE, 2010: 51-55.
[21] X. Ding, Y.-T. Zhang, Pulse transit time technique for cuffless unobtrusive blood pressure measurement: from theory to algorithm, Biomed. Eng. Lett. 9 (1) (2019) 37–52.
[22] J.M. Bote, J. Recas, R. Hermida, Evaluation of blood pressure estimation models based on pulse arrival time, Comput. Electr. Eng. 84 (2020) 106616.
[23] Y.-C. Hsu, Y.-H. Li, C.-C. Chang, L.N. Harfiya, Generalized deep neural network model for cuffless blood pressure estimation with photoplethysmogram signal only, Sensors 20 (19) (2020) 5668.
[24] N. TaheriNejad, Y. Rahmati, Blood pressure estimation using a single ppg signal, in: International Conference on Wearables in Healthcare, Springer International Publishing, Cham, 2020, pp. 3–11.
[25] L.-P. Yao, Z.-L. Pan, Cuff-less blood pressure estimation from photoplethysmography signal and electrocardiogram, Phys. Eng. Sci. Med. 44 (2) (2021) 397–408.
[26] F. Miao, B.o. Wen, Z. Hu, G. Fortino, X.-P. Wang, Z.-D. Liu, M. Tang, Y.e. Li, Continuous blood pressure measurement from one-channel electrocardiogram signal using deep-learning techniques, Artif. Intell. Med. 108 (2020) 101919.
[27] C. Sideris, H. Kalantarian, E. Nemati, et al. Building continuous arterial blood pressure prediction models using recurrent networks, in: 2016 IEEE International Conference on Smart Computing (SMARTCOMP). IEEE, 2016: 1-5.
[28] B.L. Hill, N. Rakocz, Á. Rudas, J.N. Chiang, S. Wang, I. Hofer, M. Cannesson, E. Halperin, Imputation of the continuous arterial line blood pressure waveform from non-invasive measurements using deep learning, Sci. Rep. 11 (1) (2021).
[29] A.B. Malayeri, M.B. Khodabakhshi, Concatenated convolutional neural network model for cuffless blood pressure estimation using fuzzy recurrence properties of photoplethysmogram signals, Sci. Rep. 12 (1) (2022) 6633.
[30] A.C. Tatliparmak, S. Yilmaz, Agreement of Oscillometric and Auscultatory blood pressure measurement methods: An ambulance noise simulation study, Am. J. Emerg. Med. 67 (2023) 120–125.
[31] P. McCullagh, Generalized linear models, Routledge, 2019.
[32] D.A. Nix, A.S. Weigend, Estimating the mean and variance of the target probability distribution, in: Proceedings of 1994 ieee international conference on neural networks (ICNN'94). IEEE, 1994, 1: 55-60.
[33] A.K. Menon, S. Jayasumana, A.S. Rawat, et al. Long-tail learning via logit adjustment. arXiv preprint arXiv:2007.07314, 2020.
[34] A.L. Goldberger, L.A.N. Amaral, L. Glass, J.M. Hausdorff, P.C. Ivanov, R.G. Mark, J. E. Mietus, G.B. Moody, C.-K. Peng, H.E. Stanley, PhysioBank, PhysioToolkit, and PhysioNet: components of a new research resource for complex physiologic signals, Circulation 101 (23) (2000).
[35] M. Kachuee, M.M. Kiani, H. Mohammadzade, M. Shabany, Cuffless blood pressure estimation algorithms for continuous health-care monitoring, IEEE Trans. Biomed. Eng. 64 (4) (2017) 859–869.
[36] C. Hu, F. Xing, S. Pan, R. Yuan, Y. Lv, Fault Diagnosis of Rolling Bearings Based on Variational Mode Decomposition and Genetic Algorithm-Optimized Wavelet Threshold Denoising, Machines 10 (8) (2022) 649.
[37] W. Zong, T. Heldt, G.B. Moody, et al., An open-source algorithm to detect onset of arterial blood pressure pulses, in: Computers in Cardiology. IEEE, 2003, 2003, pp. 259–262.
[38] T.Y. Lin, P. Dollár, R. Girshick, et al. Feature pyramid networks for object detection, in: Proceedings of the IEEE conference on computer vision and pattern recognition. 2017: 2117-2125.
[39] Wen Bo. Research on modeling method of cuff free blood pressure based on deep neural network[D]. University of Chinese Academy of Sciences (Shenzhen Institute of Advanced Technology, Chinese Academy of Sciences), 2020.
[40] C. Yan, Z. Li, W. Zhao, et al., Novel deep convolutional neural network for cuff-less blood pressure measurement using ECG and PPG signals, in: 2019 41st Annual International Conference of the IEEE Engineering in Medicine and Biology Society (EMBC). IEEE, 2019, pp. 1917–1920.
[41] S.S. Mousavi, M. Firouzmand, M. Charmi, M. Hemmati, M. Moghadam, Y. Ghorbani, Blood pressure estimation from appropriate and inappropriate PPG signals using A whole-based method, Biomed. Signal Process. Control 47 (2019) 196–206.
[42] S. He, H.R. Dajani, M. Bolic, Novel Cuffless Blood Pressure Estimation Method Using a Bayesian Hierarchical Model, in: 2021 43rd Annual International Conference of the IEEE Engineering in Medicine & Biology Society (EMBC). IEEE, 2021, pp. 898–901.
[43] D.U. Jeong, K.M. Lim, Combined deep CNN–LSTM network-based multitasking learning architecture for noninvasive continuous blood pressure estimation using difference in ECG-PPG features, Sci. Rep. 11 (1) (2021) 13539.
[44] E. O??Brien, J. Petrie, W. Littler, M. de Swiet, P.L. Padfield, K. O??Malley, M. Jamieson, D. Altman, M. Bland, N. Atkins, The British Hypertension Society protocol for the evaluation of automated and semi-automated blood pressure measuring devices with special reference to ambulatory systems, J. Hypertens. 8 (7) (1990) 607–619.
[45] G.S. Stergiou, B. Alpert, S. Mieke, R. Asmar, N. Atkins, S. Eckert, G. Frick, B. Friedman, T. Graßl, T. Ichikawa, J.P. Ioannidis, P. Lacy, R. McManus, A. Murray, M. Myers, P. Palatini, G. Parati, D. Quinn, J. Sarkis, A. Shennan, T. Usuda, J. Wang, C.O. Wu, E. O'Brien, A universal standard for the validation of blood pressure measuring devices: Association for the Advancement of Medical Instrumentation/European Society of Hypertension/International Organization for Standardization (AAMI/ESH/ISO) Collaboration Statement, Hypertension 71 (3) (2018) 368–374.
[46] I. Sharifi, S. Goudarzi, M.B. Khodabakhshi, A novel dynamical approach in continuous cuffless blood pressure estimation based on ECG and PPG signals, Artif. Intell. Med. 97 (2019) 143–151.
[47] S. Baek, J. Jang, S. Yoon, End-to-end blood pressure prediction via fully convolutional networks, IEEE Access 7 (2019) 185458–185468.
[48] Y.-Z. Yoon, J.M. Kang, Y. Kwon, S. Park, S. Noh, Y. Kim, J. Park, S.W. Hwang, Cuff-less blood pressure estimation using pulse waveform analysis and pulse arrival time, IEEE J. Biomed. Health Inform. 22 (4) (2018) 1068–1074.